Macromolecules

pubs.acs.org/Macromolecules Article

Simple Calibration of Block Copolymer Melt Models

Artem Petrov,* Hejin Huang, and Alfredo Alexander-Katz*

Cite This: *Macromolecules* 2024, 57, 8212–8222 Read Online

ACCESS | Metrics & More | Article Recommendations | Supporting Information

ABSTRACT: According to the universality hypothesis, the phase behavior of different block copolymer melt models having a fixed chain architecture depends solely on two parameters: the invariant chain length $\bar{N}$ and the effective interaction parameter χN. If models behave universally, they can be compared to each other and can predict experiments quantitatively. The majority of simulations, however, do not use the Flory–Huggins parameter χ directly but instead operate with the exchange energy $\alpha = \epsilon_{AB} - (\epsilon_{AA} + \epsilon_{BB})/2$, where ϵ_{xy} is the interaction energy between monomers of type x and y. The simplest Flory-like definition of χ is a standard linear relation: $\chi \propto \alpha$; however, previous studies have shown that the universality hypothesis does not hold for all models using this approximation. Here, we analyzed the behavior of more than 30 coarse-grained symmetric diblock copolymer melt models. We discovered that the phase behavior of a wide *family* of models depends only on two parameters, $\bar{N}$ and χN, if the simple linear definition of χ is imposed. This family is comprised of the models in which the monomer interaction potential energy z has a near-symmetric distribution around its mean. This phenomenon could be explained by the coincidence of normalized peak scattering intensity at the same χN and $\bar{N}$, which was observed for selected models with symmetric z-distribution when the $\chi \propto \alpha$ expression was used. Our results indicate that the main parameter controlling the symmetry of the z-distribution is the monomer density ρ. Above certain ρ, models have symmetric z-distributions, and their order–disorder transition points follow a master curve similar to the one predicted by Fredrickson–Helfand theory in the experimentally relevant $\bar{N} > 10^2$ range. On the other hand, low-ρ models exhibit skewed z-distributions, and the simple $\chi \propto \alpha$ formula is no longer universally applicable to them. We provided a table containing the linear $\chi(\alpha)$ mapping; if that mapping is used, all models with a symmetric z-distribution have the phase behavior depending solely on $\bar{N}$ and χN. Our results will enable a simple comparison between a broad family of coarse-grained models and experiments and can guide block copolymer model building. This, in turn, will facilitate the screening of new block copolymer morphologies and support material design.

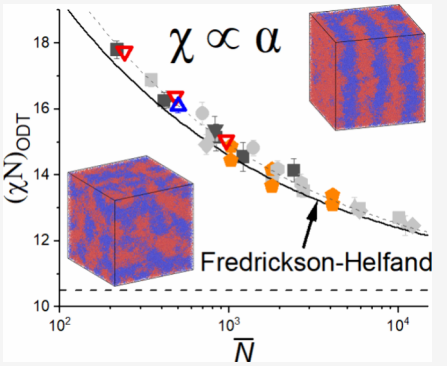

1. INTRODUCTION

Melts consisting of block copolymers are able to form ordered microphases in which the monomers of different types are distributed periodically in space. Such structures have immense importance in nanotechnology applications, especially in nanophotonics, green plastics, and nanolithography.[1] The simplest example of a block copolymer is a symmetric diblock copolymer that consists of two A and B blocks having equal volume fractions. Such polymers are able to self-assemble into nanometer-scale periodic lamellar structures at the so-called order–disorder transition (ODT) temperature. Predicting the location of the ODT point from the physicochemical properties of polymers, which is crucial for building a phase diagram of any block copolymer material, still remains an unsolved problem despite the simplicity of this polymer system and five decades of research.[2]

The classical measure of dissimilarity between the monomers of type A and B is the Flory–Huggins parameter χ; it characterizes the positive enthalpic contribution to the free energy of a block copolymer melt.[3] Both Leibler's incompressible fourth-order random phase approximation (RPA) theory and the self-consistent (mean) field theory (SCFT) predicted that the product of χ at ODT and the chain degree of polymerization N equals to a single number $(\chi N)_{ODT} = 10.495$.[3] However, these theories disregarded density fluctuations at scattering vectors different from the instability vector near the ODT point; as a result, SCFT is expected to work only for infinitely long polymers.[4]

We can characterize how close a certain system is to the mean-field SCFT regime by the invariant chain length $\bar{N} = (\rho R^3/N)^2$, which plays the role of the Ginzburg parameter,[5] where ρ is the monomer concentration (the number of monomer units per unit volume), and R is the mean end-to-end distance of a copolymer. After the seminal work of Leibler, a number of researchers attempted to take density fluctuations at ODT into account more correctly. Following Brazovskii,[6] the first theory that included fluctuations was developed by

Received: March 26, 2024
Revised: July 5, 2024
Accepted: August 6, 2024
Published: August 14, 2024

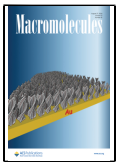

https://doi.org/10.1021/acs.macromol.4c00680
Macromolecules 2024, 57, 8212–8222

Fredrickson and Helfand (FH)[7] and corrected by Olvera de la Cruz (OC) and co-workers.[8] They found that the $(\chi N)_{\mathrm{ODT}}$ value for finite symmetric diblock copolymers should be larger than the SCFT prediction as

$$(\chi N)_{\mathrm{ODT}} = 10.495 + 41.0\bar{N}^{-1/3} \quad (1)$$

The FH theory was supported by several experimental works.[9−11]

In the last few decades, with the advent of fast computers, a lot of attention in polymer science was attracted to computer simulations. Modeling provides researchers with an inexpensive way to study the complex phase behavior of block copolymers at the most detailed level. However, the biggest challenge arising when one tries to compare the results of a simulation to an experiment is the difficulty of mapping the simulation parameters onto experimentally measurable quantities. For instance, the χ parameter, which is utilized in experiments to control the miscibility of A and B blocks, is not used as an input parameter in most simulations. In field-theoretic modeling, a "bare" interaction parameter χ_b is adjusted; in particle-based simulations, the exchange energy $\alpha = \epsilon_{AB} - (\epsilon_{AA} + \epsilon_{BB})/2$ is varied. The χ parameter is a monotonically increasing function of either χ_b or α; however, there exists a plethora of mappings between these quantities.[5,12−20] The most widely used relation is a simple linear approximation $\chi = z_{mod}\alpha/k_B\mathrm{T}$, where T is temperature and z_{mod} is a model-dependent prefactor characterizing the monomer coordination number.[5,12,21−23] This linear approximation is expected to be true in the limit of small α; at large α, nonlinear terms are permissible in principle.[17−20,22] This natural approximation has a clear physical meaning: the free energy of interaction per monomer is proportional to the potential energy of a monomer−monomer contact. Another great virtue of this relation is its direct applicability to various types of block copolymers.

However, it turned out that this approximation had a serious disadvantage. Several simulation works[5,21,24] pointed out that if the $\chi \propto \alpha$ expression was assumed, the $(\chi N)_{\mathrm{ODT}}$ values depended not only on $\bar{N}$ but also on other model details that do not have strict correspondence to the characteristics of real polymer systems. Moreover, when the $\chi \propto \alpha$ formula was used, the excess free energy per chain and the peak of the invariant structure factor did not depend solely on χN and $\bar{N}$, contrary to the expectations. In other words, the $\chi \propto \alpha$ approximation yielded a so-called "nonuniversal" behavior of polymer models at ODT, which hampered the comparison of simulations to experiments. This effect was observed for the values of $\bar{N}$ that are usually achieved experimentally: $10^2 < \bar{N} < 10^4$.

The solution to this problem was found by Morse and co-workers[5,21] who showed that a *nonlinear* $\chi(\alpha)$ relation leads to the universal $(\chi N)_{\mathrm{ODT}}(\bar{N})$ dependency for a variety of particle-based models. Moreover, they demonstrated that the $(\chi N)_{\mathrm{ODT}}$ values were substantially larger than the FH prediction in the range $10^2 < \bar{N} < 10^4$ (eq 2).

$$(\chi N)_{\mathrm{ODT}} = 10.495 + 41.0\bar{N}^{-1/3} + 123.0\bar{N}^{-0.56} \quad (2)$$

Later, Matsen and co-workers found that the same formula predicted well the $(\chi N)_{\mathrm{ODT}}$ values in field-theoretic simulations if χ was allowed to be a nonlinear function of χ_b.[25,26]

This nonlinear $\chi(\alpha)$ relation is model-specific and can be found from mapping the peak of the structure factor in the disordered phase of a diblock copolymer melt model to the universal function predicted by the renormalized one-loop (ROL) theory.[4,27,28] One of the downsides of this mapping is that it is rather difficult to perform: it requires simulation of the systems and the measurement of the structure factor at different values of α and N as well as solving complex integrals numerically in addition to the determination of the z_{mod} parameter described above. Moreover, strictly speaking, ROL theory has only been developed for binary blends and diblock copolymers; it is still an open question whether the current form of the theory is applicable to other types of block copolymers which, in turn, are of much interest and technological importance. In addition, the physical nature of the nonlinear terms in $\chi(\alpha)$ is still unclear.

As a result, the majority of simulation works currently operate with the simple $\chi \propto \alpha$ expression[15,29−34] despite the issues with unphysical model-dependent behavior of simulated systems and the lack of understanding of when this formula is applicable, i.e., whether the nonlinear corrections predicted by lattice cluster theory (LCT)[17−20] and allowed by ROL theory[21,22] can be neglected for practical applications in a certain subset of models. This question arises in the light of the LCT which analytically derived the nonlinearities and showed that they vanish at small α (i.e., they vanish at ODT for the models with long chains and/or with a high coordination number if it scales inversely with α). However, it is hard to employ this theory directly to quantitatively evaluate the magnitude of $\chi(\alpha)$ nonlinearities in different models, since (i) it was quantitatively developed only for hypercubic lattices and (ii) it does not capture the dominant $\propto 1/N^{1/2}$ correction to the free energy of mixing.[22] On the other hand, ROL theory does not predict the nonlinear corrections analytically and gives the $\chi(\alpha)$ function through the complex procedure described in the previous paragraph, although allowing the linear $\chi \propto \alpha$ growth if $\alpha \ll (\epsilon_{AA} + \epsilon_{BB})/2$ in some models.[35] At the same time, modern experimental research groups, which do not have expertise in the peculiarities of ROL theory, tend to perform block copolymer simulations to gain more detailed insight into the observed phenomena.[36−39] This emphasizes the need for the method of deriving the $\chi(\alpha)$ function which (i) is as simple and general as possible and (ii) yields the phase behavior (characterized by the phase transition points and/or the free energy function) that depends only on chain architecture, $\bar{N}$, and χN, and not on other model parameters.

Here, we propose a solution to this problem. We show that the simplest $\chi \propto \alpha$ approximation, which does not require the structure factor fitting, leads to such phase behavior in a wide class of block copolymer melt models in which the effective coordination number $z(N)$ has a (quasi) *symmetric* distribution around its mean. $z(N)$ represents the dimensionless potential energy exerted on a monomer by other polymer chains of length N;[22] this quantity determines the prefactor in the $\chi = z\alpha/k_BT$ expression as $z = z(N \to \infty)$. In turn, the $z(N)$-distribution is nearly symmetric if model density is large enough. In addition, the normalized peak scattering intensity coincided for selected models belonging to this class at similar $\bar{N}$ and χN if χ was defined as $\chi = z\alpha/k_BT$. This, in turn, can explain the aforementioned phase behavior. Moreover, we found that the $(\chi N)_{\mathrm{ODT}}(\bar{N})$ master curve exhibited by such models has the functional form of the FH−OC model and is rather close to the original prediction by Fredrickson and Helfand (eq 1) and not to the expression of Morse et al. (eq 2) for $\bar{N} > 10^2$. Thus, it will be beneficial to utilize the models having symmetric $z(N)$-distribution in the future research on

https://doi.org/10.1021/acs.macromol.4c00680
Macromolecules 2024, 57, 8212−8222

Table 1. Parameter Ranges of the Studied Models: Freely-Jointed Chains (FJC), Gaussian Chains (G), Multiple- and Single-Occupancy Lattice Models,[a] and Field-Theoretic Simulations (FTS)[b]

model	ρ	N	K	r_0	$\bar{N}$
FJC	[3−20]	[20−80]	100.0	[0.7−1.31]	$(3 \times 10^2 - 1.2 \times 10^4)$
G	[1.5−15]	[16−80]	[0.867−4.0]	0.0	$(2 \times 10^2 - 4 \times 10^3)$
lattice, mult.	2.4	[16−100]	∞	$\sqrt{2}$	$(9 \times 10^2 - 6 \times 10^3)$
lattice, single	0.4	[30−180]	∞	$\sqrt{2}$	$(1 \times 10^2 - 9 \times 10^2)$
FTS	8.0	[16−64]	N/A	N/A	$(1 \times 10^3 - 5 \times 10^3)$

[a]Data taken from ref 14 and ref 21, respectively. [b]Data taken from refs 25 and 26.

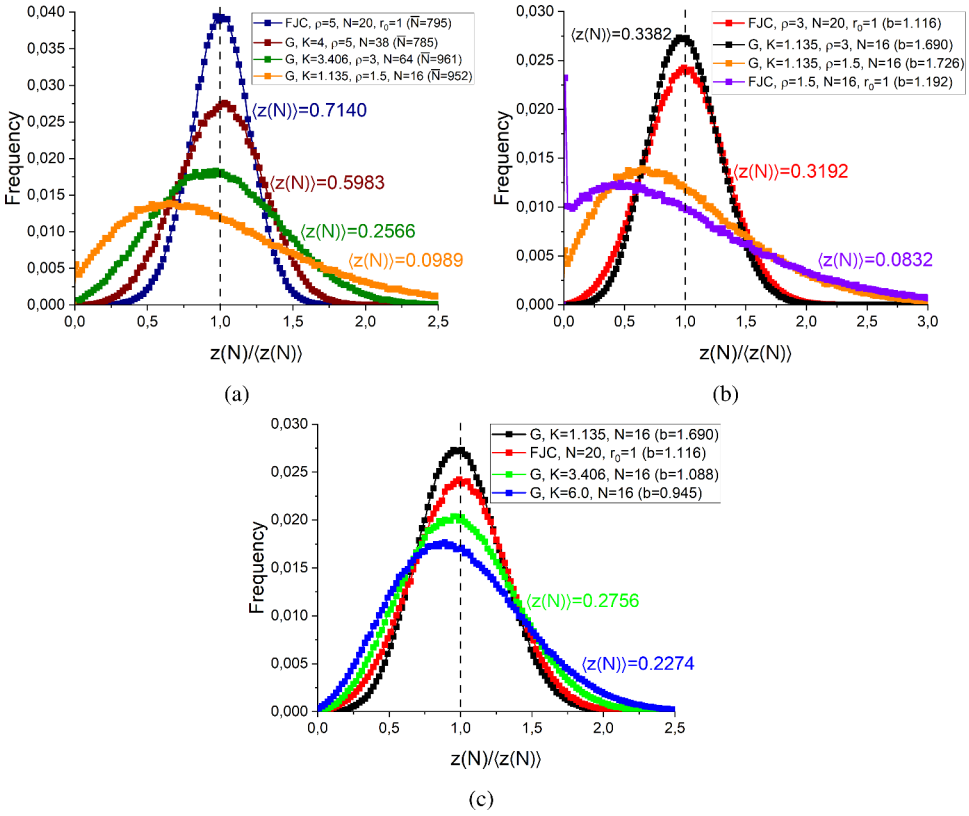

Figure 1. Distribution of $z(N)$ in different models of homopolymer melts. The $z(N)$ values were divided by the average $z(N)$ value $\langle z(N)\rangle$ for each model. Values of $\langle z(N)\rangle$ are included in the plots. The vertical dashed line shows $z(N)/\langle z(N)\rangle = 1$. Model parameters are included in the legends, and curves having same colors in different graphs correspond to the same system. (a) Models having similar values of $\bar{N}$. (b) Models having different densities ρ. The statistical segment length b for each model is listed in the parentheses. (c) Models having different values of b at the same $\rho = 3$.

phase separation of block copolymers, since such models will not require the complex nonlinear renormalization of χ and will give physically correct results even for polymers with moderate $\bar{N}$. As a result, it will be possible to compare the phase behavior and mesoscale structure of models belonging to this class easily. Moreover, one can determine the experimental $\chi(T) = A/T + B$ function for symmetric diblocks of a certain monomer chemistry directly from the master curve equation $(\chi N)_{\mathrm{ODT}}(\bar{N})$ as done in ref 9. After this, if one matches $\bar{N}$ in an experimental melt of the same chemistry and in a model with symmetric $z(N)$-distribution, it will be possible to relate the energy α in simulations to temperature T in experiments using the $T = A/[z\alpha/(k_B T) - B]$ formula. As a result, one could compare the simulations of the models with symmetric $z(N)$-distributions to experiments easily without performing the nonlinear ROL-theoretic $\chi(\alpha)$ calibration.

2. METHODS

We modeled symmetric diblock copolymer melts using dissipative particle dynamics (DPD) in NVT ensemble and a bead-and-spring representation of polymers.[12] Soft-core repulsion forces $\mathbf{F}_{ij}^c$ acted between all beads and defined the A-B repulsion energy α. In DPD, the repulsive forces are short-ranged and act only if particles are located closer than a certain cutoff distance:

$$\mathbf{F}_{ij}^c = \begin{cases} a_{xy}(1 - r_{ij})\dfrac{\mathbf{r}_{ij}}{r_{ij}}, & r_{ij} \le 1 \\ 0, & r_{ij} > 1 \end{cases} \tag{3}$$

Here, a_{xy} is the repulsion parameter between beads i and j having types x and y, respectively ($x = A,B$, $y = A,B$). In this notation, $\alpha = a_{AB} - a_{xx}$, since $a_{xx} = a_{AA} = a_{BB}$.

Chain connectivity was modeled using a harmonic spring force $\mathbf{F}_{ij}^b$ as

https://doi.org/10.1021/acs.macromol.4c00680
Macromolecules 2024, 57, 8212−8222

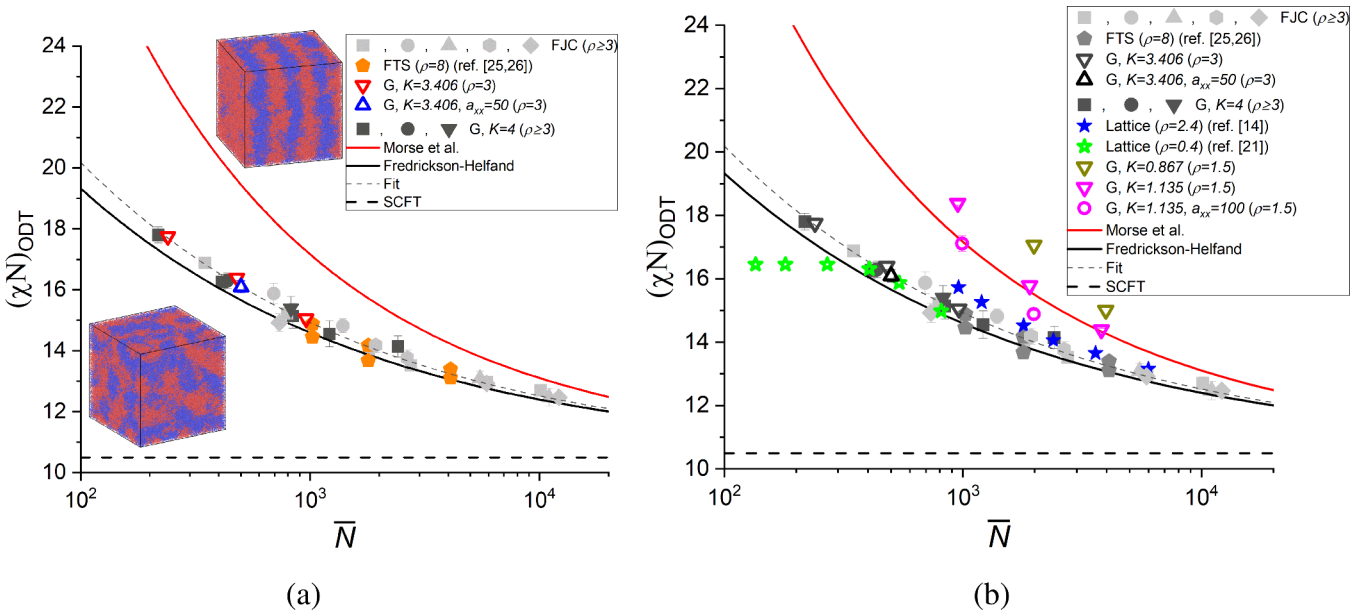

Figure 2. Order−disorder transition points ($(\chi N)_{ODT}$) of symmetric diblock copolymer melt models having different $\bar{N}$. Red, black, and thick dashed curves represent the predictions of eqs 2, 1, and SCFT, respectively. (a) The data for the models having symmetric $z(N)$-distribution. Snapshots show the disordered (bottom) and ordered (top) states near ODT for the FJC model with $\rho = 3$, $N = 80$. Data for field-theoretic simulations (FTS) are taken from refs 25 and 26. (b) The data for all studied models. The models having symmetric $z(N)$-distribution (data from (a)) are shown in gray, colored triangles and circles represent DPD models with skewed $z(N)$-distributions. The data for multiple- and single-occupancy lattice models are taken from ref 14 and ref 21, respectively. Table S1 contains correspondence between the symbol shape and the set of model parameters. Separate $(\chi N)_{ODT}(\bar{N})$ plots for each class of models are shown in Figure S4. Error bars for $\bar{N}$ are within the symbol size for all models. Error bars of $(\chi N)_{ODT}$ represent the width of the hysteresis of transition, i.e., the difference between the lowest and the highest values of χN leading to spontaneous ordering and disordering, respectively (see SI section 3). The error of determination of z is much smaller than the hysteresis width.

$$\mathbf{F}_{ij}^{b} = -K(r_{ij} - r_0)\frac{\mathbf{r}_{ij}}{r_{ij}} \tag{4}$$

Here, $\mathbf{r}_{ij}$ is the vector between beads i and j (bonded beads only for eq 4), and K is the bond stiffness. A full description of the simulation procedure is given in the Supporting Information (SI) section 1. For freely jointed chain models (FJC), which have a nonzero bond rest length r_0, we chose a stiff spring with $K = 100$,[29,40] while for "Gaussian chain" models we varied K from $K = 0.867$ to $K = 4.0$ with $r_0 = 0$. The soft-spring Gaussian models are traditionally used in particle-based simulations.[5,41] We constructed 33 DPD models of symmetric diblock copolymers by varying different simulation parameters (excluding a_{AB}, which was varied for each model to change α). The varied parameters included N, ρ, r_0, K, and the a_{xx} parameter that controlled the compressibility of a system (see SI section 1 for details). All our models had experimentally relevant invariant chain length values $10^2 < \bar{N} < 10^4$ (Table 1). We calculated $\bar{N}$ according to the definition $\bar{N} = N(\rho b^3)^2$, where ρ is the number of beads per unit volume and b is the statistical segment length determined from extrapolating the radius of gyration $R_g^2 = N\,b^2/6$ to $N \to \infty$ (see SI section 2). The full set of parameters for each model is given in Table S1. To support our conclusions, we also compared our results to the previously published data on the following non-DPD models of symmetric diblock copolymer melts: (i) field-theoretic simulations (FTS),[25,26] which used the standard Gaussian model of polymer chains,[42] and (ii) lattice models with single or multiple occupancy of a lattice site.[14,21] Table 1 includes ranges of parameters for all studied models.

3. RESULTS

3.1. $z(N)$-Distributions. Before studying the disorder-to-lamellae phase transition (ODT), we investigated the $z(N)$-distributions of the DPD models at $\chi = 0$ (i.e., fully homogeneous phase). $z(N)$ is proportional to the potential energy of interaction of a bead with other chains; $z(N)$ characterizes the effective coordination number of each bead and the $z(N)$-distribution shows how this quantity fluctuates from bead to bead at any given time or, conversely, how $z(N)$ fluctuates for a single bead in time. For the DPD interaction potential (eq 3), $z(N)$ was calculated for each bead i at a given time according to eq 5.

$$z(N) \equiv z_i(N) = \sum_j 0.5(1 - r_{ij})^2 \tag{5}$$

Here, the distance between beads is $r_{ij} < 1$ (i.e., the sum in eq 5 includes only those neighbors of the bead i that are located within the interaction force cutoff in eq 3). The beads i and j cannot belong to the same chain. The data for the distribution was collected over all beads in the system and over 10 structures obtained every 10^5 DPD time steps after equilibration. The system-averaged value of $z(N)$ was determined as $\langle z(N)\rangle_{syst} = \sum_i z_i(N)/(NM)$, where M is the total number of chains in the system; $\langle z(N)\rangle_{syst}$ was then time-averaged across the analyzed 10 structures to obtain the final averaged $z(N)$ value denoted as $\langle z(N)\rangle$.

To evaluate whether the parameters of models had any effect on the $z(N)$-distribution, we constructed four different models having roughly similar $\bar{N}$. Figure 1a shows that the distributions behaved qualitatively differently depending on the model. For the high-density FJC and Gaussian models, the distributions of $z(N)$ had symmetric, near-Gaussian form. However, upon a decrease of system density below $\rho \approx 3$, the distributions became strongly skewed.

To investigate the effect of the model parameters on the skew of the distributions in more detail, we analyzed the two sets of models having different ρ but similar b, K, and N. Figure

https://doi.org/10.1021/acs.macromol.4c00680
Macromolecules 2024, 57, 8212−8222

1b demonstrates that a decrease of density led to a strong skew of the distributions regardless of the chain model (FJC or Gaussian). Figure 1c shows that a decrease of the bond length at moderate density $\rho = 3$ also led to a slight skew of the $z(N)$-distribution, although b affected the skew much more weakly than ρ (Figure 1b). Finally, making systems more compressible (decreasing a_{xx}) also led to slightly more skewed $z(N)$-distributions (Figure S2a).

This behavior can be explained by examining the microscopic structure of a simple DPD liquid. A decrease of ρ leads to a decrease in the number of neighbors around a monomer (Figure S2d), which causes a decrease of $\langle z(N)\rangle$. At some low ρ, beads with zero neighbors (i.e., with $z(N) = 0$) appear in the system, and the average number of neighbors k becomes very small ($k \approx 5$ at $\rho = 1.5$, Figure S2d). This, in turn, makes $z(N)$ fluctuate strongly from bead to bead due to a small number of summands in eq 5, thus increasing the relative spread of the $z(N)$-distribution (Figure S2b). These strong fluctuations of $z(N)$, combined with a small average $z(N)$, give rise to a right-skewed $z(N)$-distribution due to the nonnegativity of $z(N)$ (Figure S2b). In a polymer liquid, a bead experiences fewer contacts with monomers from other chains upon a decrease of density or bond length (Figure 1, S2c, S9). As a result, the $z(N)$-distribution becomes skewed at low ρ and b (Figure 1b,c). Compressibility of the system also has an effect since less compressible systems have narrower and, therefore, less skewed $z(N)$-distributions (Figure S2a). However, despite an abundance of parameters defining the shape of the $z(N)$-distribution, the system density plays the dominant role as shown in Figure 1b. We can confirm these qualitative considerations quantitatively by constructing a simple analytical theory that describes the skewness of the $z(N)$-distributions in the models with DPD-like interaction potential (eq 3) (see SI section 6). One of the main assumptions underlying the theory states that the summands in eq 5 are independent random variables, which should be true for very small and very large k. Our theory predicts that the skewness is primarily controlled by k and decreases as the skewness of gamma distribution: skewness $= 2/\sqrt{k}$, which was confirmed by the data for the small- and large-k models. The number k, in turn, is mostly defined by ρ; for DPD models, $k \approx 3.95\rho$. An increase of b also slightly increases k, which decreases the skewness (Figure 1c).

3.2. Phase Behavior of Models. Next, we studied how the $z(N)$-distribution affected the behavior of systems at ODT. We established the ODT point location $(\chi N)_{\mathrm{ODT}}(\bar{N})$ for all studied models. We assumed the linear relation between χ and α ($\chi = z\alpha/k_BT$). Following Morse and co-workers,[21] the value of z was calculated for each model as the $N \to \infty$ limit of $\langle z(N)\rangle$ measured at $\chi = 0$ using an analytical ROL-theoretic expression (see SI section 2). Such an approach provides the dominant linear term in the $\chi(\alpha)$ function, since the ROL theory yields the dominant $\propto 1/N^{1/2}$ correction to the free energy of mixing.[22] To determine $(\chi N)_{\mathrm{ODT}}$ as $(\chi N)_{\mathrm{ODT}} = zN\alpha_{\mathrm{ODT}}/k_BT$, we established α_{ODT} as the average between the lowest and highest values of α leading to ordering and disordering, respectively (see SI section 3).

Our main results are presented in Figure 2. Figure 2a shows the $(\chi N)_{\mathrm{ODT}}(\bar{N})$ dependency for all models having nearly symmetric distribution of $z(N)$. We included the field-theoretic simulation (FTS) data in Figure 2a, since ref 43 demonstrated that the microscopic field distribution, proportional to $z(N)$, is symmetric in FTS at the studied values of $\bar{N}$. Figure 2a shows that all $(\chi N)_{\mathrm{ODT}}$ values obtained at a similar invariant chain length $\bar{N}$ overlapped within the error of $(\chi N)_{\mathrm{ODT}}$ determination. In other words, if one assumes the simplest linear $\chi \propto \alpha$ relation, the phase transition point will depend only on $\bar{N}$ for all models with nearly symmetric $z(N)$-distributions. Furthermore, this conclusion holds at high enough ρ even if the *pressure* is held constant for a given model instead of ρ (see SI section 7) as done in molecular dynamics simulations in ref 21. Moreover, fitting of the DPD simulation data in Figure 2a by the expression $(\chi N)_{\mathrm{ODT}} = 10.495 + A\,\bar{N}^{-B}$ yielded $A = 46.4 \pm 2.3$ and $B = 0.340 \pm 0.008$ (thin gray dashed curve). Therefore, the exponent B coincided with the exponent predicted by the FH theory (eq 1) within the error. The prefactor A differed by ≈12% from the FH-theoretic prefactor 41.0. As a result, the master curve exhibited by the data resembled eq 1, demonstrating an interesting qualitative agreement with the classical theory which, however, is strictly valid for much greater values of $\bar{N}$.[7]

Figure 2b shows the $(\chi N)_{\mathrm{ODT}}(\bar{N})$ dependencies for all studied models. The DPD models having skewed $z(N)$-distributions showed nonuniversal behavior in the $\chi \propto \alpha$ approximation and did not follow eq 1 or 2. We investigated how the $z(N)$-distribution skew affected the deviation from the master curve exhibited by the models with nearly symmetric $z(N)$-distributions by decreasing the model compressibility 4-fold (the parameter a_{xx} was increased from $a_{xx} = 25$ to $a_{xx} = 100$ for the Gaussian models with $K = 1.135$ and $\rho = 1.5$). Figure 2b shows that less compressible models (open magenta circles) had $(\chi N)_{\mathrm{ODT}}$ points lying closer to the master curve compared to the more compressible models (open magenta triangles); on the other hand, these less compressible models had more symmetric $z(N)$-distributions (Figure S2a). Therefore, a decrease of the $z(N)$-distribution skew can drive models toward the regime in which their phase behavior depends solely on $\bar{N}$ and χN in the $\chi \propto \alpha$ approximation. In contrast, an increase of the a_{xx} parameter for a system with symmetric $z(N)$-distribution (Gaussian model with $K = 3.406$, $\rho = 3$, $N = 32$, blue triangle in Figure 2a) did not influence $(\chi N)_{\mathrm{ODT}}$ strongly. In other words, we observed that the master $(\chi N)_{\mathrm{ODT}}(\bar{N})$ curve formed by the models with symmetric $z(N)$-distributions in the $\chi \propto \alpha$ approximation is invariant under the change of their compressibility as opposed to the models with skewed $z(N)$-distributions.

Next, we studied the previously published data for single- and multiple-occupancy lattice models with the average polymer density $\rho = 0.4$ and $\rho = 2.4$, respectively.[14,21] Both models used face-centered-cubic lattice. A monomer in the single-occupancy model[21] interacted with all 12 neighboring lattice sites; however, the average number of other-chain neighbors was closer to ≈8 due to the presence of the same-chain neighbors and vacancies (20% of all sites). We do not have access to the $z(N)$-distribution for those models; however, in the long chain limit ($N \geq 90$), the single-occupancy lattice models followed the same master curve formed by the DPD models with symmetric $z(N)$-distributions for $\bar{N} \gtrsim 400$ (Figure 2b). The deviation from the master curve occurred in the small- $\bar{N}$ limit similarly to ref 21 presumably due to the short-chain effects and a possible $z(N)$-distribution skew. The multiple-occupancy lattice models[14] used a Hamiltonian that considered only same-site interactions. Therefore, and contrary to our intuition, the average number of other-chain contacts per monomer was at most ≈4. Thus, the effect of the small number of neighbors on the $z(N)$-

https://doi.org/10.1021/acs.macromol.4c00680
Macromolecules 2024, 57, 8212−8222

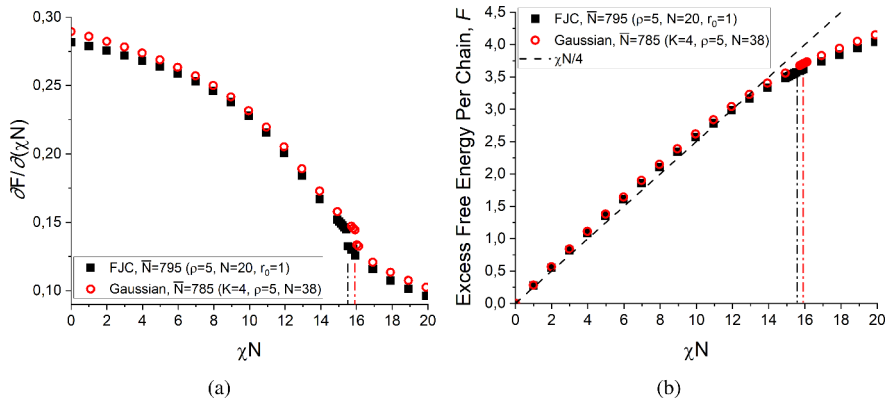

Figure 3. (a) The χN-dependencies of the first derivative of the excess free energy per chain for an FJC model (black dots) and for a Gaussian model with $K = 4$ (red circles); both models had symmetric z(N)-distributions and a similar $\bar{N} \approx 800$. Both dependencies exhibited a discontinuity at ODT: vertical dash-dotted lines represent the lowest possible χN values at which ordering occurred for the FJC model (black) and for the Gaussian model (red). In both models, $(\chi N)_{ODT}$ values coincided within the error associated with the hysteresis of transition. (b) The dependencies of the excess free energy per chain in the two models calculated by numerically integrating (a). The black dashed line shows the mean-field dependency in the disordered phase ($F = \chi N/4$).

distribution skew might be significant in those models. These multiple-occupancy lattice models adhered to the master curve at high $\bar{N}$ but started to deviate from it at $\bar{N} \lesssim 10^3$ (Figure 2b). We conjecture that this deviation would disappear if the Hamiltonian of those multiple-occupancy models additionally included the interaction between the neighboring lattice sites, which would include more neighbors in the $z(N)$ calculation. It is worth mentioning that other studies pointed out the importance of the number of monomer neighbors in the on- and off-grid multiple-occupancy models.[44−46] For instance, ref 44 indicated that packing stops affecting the χ parameter if a bead interacts with over 10 neighbors. We did not include the data from ref 44 to Figure 2b, since the authors of this study did not calculate the z parameter according to the ROL theory (as done for all models in Figure 2).

Finally, researchers studied models with a hard-core Lennard-Jones interaction potential.[21,47] One of these models having $\rho = 0.7$ exhibited strong nonuniversal behavior in the $\chi \propto \alpha$ approximation.[21] We expect this system to have a strongly skewed $z(N)$-distribution due to a very low density that yields strong packing (structural) effects.[44] Thus, we do not expect such low-density systems to ever have phase behavior dependent only on $\bar{N}$ and χN in the $\chi \propto \alpha$ mapping except for the models with very long chains; the modeling of such systems, however, is computationally unfeasible due to long relaxation times.

We also confirmed that the phase behavior of models with symmetric $z(N)$-distributions depends solely on $\bar{N}$ and χN in the $\chi \propto \alpha$ approximation from a different perspective. We analyzed the χN-dependencies of the excess free energy per chain and its first derivative (Figure 3). The derivative (Figure 3a) was estimated as $\partial F/\partial(\chi N) = u_{AB}/z a_{AB} k_B T$ (see ref 21). Here, $u_{AB}(\chi N)$ is the average potential energy of A-B nonbonded interaction per bead measured at a given χN; $a_{AB}(\chi N)$ is the AB-repulsion energy coefficient determining χ (eq 3). The free energy (Figure 3b) was calculated by the numerical integration of the first derivative. We calculated the dependencies for two models having symmetric $z(N)$-distributions and similar $\bar{N}$. First, the excess free energy agreed well with the mean-field disordered state dependency $F = \chi N/4$ below the ODT point (to the left of the vertical lines in Figure 3b), as expected. For higher χN, the systems became ordered, and the excess free energy deviated from the $F = \chi N/4$ line, also according to the qualitative expectations. Second, we found that the excess chain free energy and its first derivative agreed well at similar $\bar{N}$ for all χN values up to and above the ODT. These data confirmed that the models with symmetric $z(N)$-distribution have phase behavior (which is determined by the free energy) dependent solely on $\bar{N}$ and χN in the linear $\chi \propto \alpha$ approximation.

3.3. Invariant Structure Factor. Finally, we measured the invariant structure factor $S(q)/(\rho N)$, which characterizes composition fluctuations in a copolymer melt. This quantity should not depend on the definition of a "monomer" in a polymer model. Therefore, for symmetric diblock copolymers, $S(q)/(\rho N)$ is predicted to depend only on χN, $\bar{N}$, and the normalized wavenumber qR_{g0}, where R_{g0} is defined as $R_{g0} = b(N/6)^{1/2}$.[3,35] The scattering intensity $S(q)$ is defined as the Fourier transform of the pair correlation function of composition fluctuations[35] (eq 6).

$$S(\mathbf{q}) = \frac{1}{4}\int \mathrm{d}\mathbf{r} e^{i\mathbf{q}\mathbf{r}} \langle (\rho_A(\mathbf{r}) - \rho_B(\mathbf{r}) + (1-2f)\rho)(\rho_A(\mathbf{0}) - \rho_B(\mathbf{0}) + (1-2f)\rho)\rangle \quad (6)$$

Here, $\rho_A(\mathbf{r})$ and $\rho_B(\mathbf{r})$ are concentrations of beads of type A and B at point $\mathbf{r}$, respectively, and f is the composition of a block copolymer ($f = 0.5$ in this work). eq 6 can be rewritten in a more convenient discrete form, which we used for the calculation of $S(q)$ in our DPD simulations (eq 7, also see ref 48).

$$S(\mathbf{q}) = \frac{\rho}{4N_{\mathrm{part}}}\left|\sum_{i=1}^{N_{\mathrm{part}}} e^{i\mathbf{q}\mathbf{r}_i} b_i\right|^2 \quad (7)$$

In eq 7, N_{part} is the total number of beads in a simulation box; b_i equals to 1 or −1 if the i-th bead has type A or B, respectively. The structure factor $S(q)$ was obtained by averaging $S(\mathbf{q})$ over all vectors $\mathbf{q}$ having the same length $|\mathbf{q}| = q$ and over 100 structures obtained after melt equilibration every 5×10^4 DPD time steps.

We measured $S(q)$ in the disordered state for two models having symmetric $z(N)$-distributions and similar $\bar{N}$. We analyzed the two models characterized in the previous section

https://doi.org/10.1021/acs.macromol.4c00680
Macromolecules 2024, 57, 8212−8222

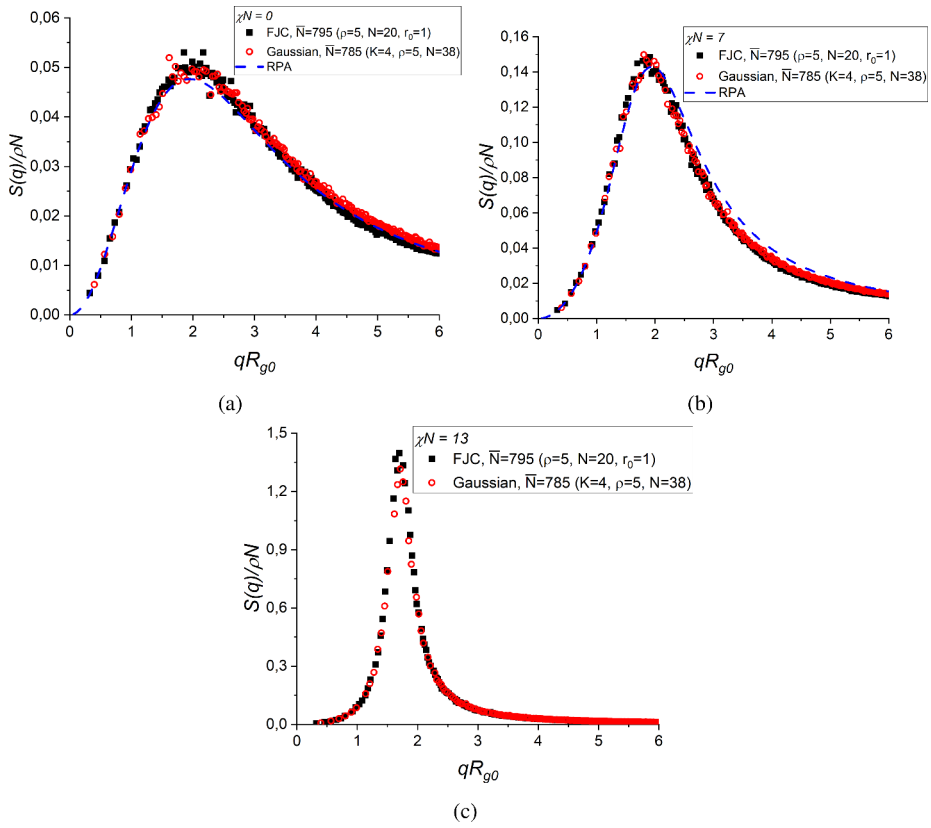

Figure 4. Dependency of the normalized structure factor $S(q)/(\rho N)$ on the rescaled wavenumber qR_{g0} for two different models of diblock copolymer melts with symmetric $z(N)$-distribution having similar $\bar{N} \approx 800$. The RPA predictions for $S(q)/(\rho N)$ are shown by the blue dashed curves.[3] (a) $\chi N = 0$, (b) $\chi N = 7$, and (c) $\chi N = 13$.

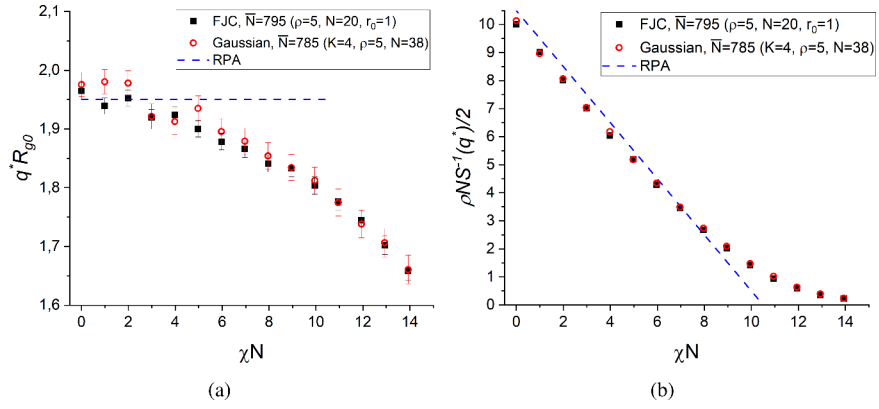

Figure 5. Dependencies of (a) the peak wavenumber and (b) the inverse peak scattering intensity on χN for the two models with symmetric $z(N)$-distributions. The RPA predictions are shown by the blue dashed lines. The error of q^*R_{g0} was estimated using the formula $\sigma_{q^*R_{g0}} = \pi^2 R_{g0}/(L^2 q^*)$ obtained using the linear uncertainty propagation theory and using the following estimation for the q^2 uncertainty: $\sigma_{q^2} = 0.5(2\pi/L)^2$, where L is the simulation box side length.

in Figure 3: an FJC model with $N = 20$, $\rho = 5$, and $r_0 = 1.0$, and a Gaussian model with $N = 38$, $K = 4.0$, and $\rho = 5$. Invariant structure factors measured for the two models at different χN are shown in Figure 4. We see that the $S(q)/(\rho N)$ dependencies agreed very well in the two models for all χN. The best agreement was observed at sufficiently large length scales ($qR_{g0} \lesssim 4$) similar to the observations in ref 35; therefore, the mesoscopic structure of the two models having symmetric $z(N)$-distributions is almost identical at similar $\bar{N}$ and χN (even if the $\chi = z\alpha/k_BT$ definition is assumed). At smaller length scales, the structure factors started to deviate, as expected, due to the different microscopic structure of the two models.

In addition, we can characterize the mesoscopic structure by analyzing the peak wavenumber q^*R_{g0} and the peak scattering intensity $S(q^*)/(\rho N)$ (Figure 5a,b). Both of these quantitites were obtained via fitting the $S(q)/(\rho N)$ dependencies in the $qR_{g0} \in [1,3]$ range with a smooth function as described in ref 35. q^*R_{g0} and $S(q^*)/(\rho N)$ were determined as the peak x- and y-coordinates of the fitted function, respectively; fits were performed for $\chi N \leq 14$, since the fitting was unreliable for higher χN due to the proximity to ODT. Figure 5a shows that

https://doi.org/10.1021/acs.macromol.4c00680
Macromolecules 2024, 57, 8212−8222

the q^*R_{g0} values agreed well with the RPA prediction $q^*R_{g0} \approx 1.95$ at small χN and decreased at higher χN due to finite-$\bar{N}$ effects in agreement with previous studies.[35] Moreover, $q^*R_{g0}(\chi N)$ dependencies agreed for both models almost perfectly within the error of q^* that stemmed from the finite simulation box size. This fact confirmed the qualitative observations in Figure 4: in the two models with symmetric $z(N)$-distributions, the characteristic composition fluctuation scale depends only on χN for the same $\bar{N}$ if the $\chi = z\alpha/k_BT$ formula is adopted.

Figure 5b shows that the $\rho NS^{-1}(q^*)/2$ values were slightly smaller than the RPA prediction $10.5-\chi N$ at small χN; at $\chi N \gtrsim 9$, the measured values exceeded the RPA prediction, in full agreement with the previous simulation and theoretical results.[21,35] Most importantly, the $\rho NS^{-1}(q^*)(\chi N)$ dependencies coincided perfectly for both models having symmetric $z(N)$-distributions when the $\chi = z\alpha/k_BT$ expression was used. Interestingly, both models had rather short chains: $N = 20$ and $N = 38$ for FJC and Gaussian models, respectively. In turn, an increase of N leads to a better agreement of the peak scattering intensity in different models with the same $\bar{N}$.[16,21] Therefore, FJC models with $\rho = 5$, $r_0 = 1.0$, and $N \geq 20$ are expected to have the same peak scattering intensity as the Gaussian models with $K = 4.0$, $\rho = 5$, and $N \geq 38$ (at the same χN and $\bar{N}$). This conclusion suggests that using the $\chi = z\alpha/k_BT$ expression is enough to yield the agreement between the $\rho NS^{-1}(q^*)(\chi N)$ dependencies measured in the aforementioned FJC and Gaussian models at various N in the characteristic range $N \in (10^1, 10^2)$. Reaching the same agreement in a similar N-range was the purpose of the nonlinear $\chi(\alpha)$ mapping procedure developed in refs 5, 16, 21, and 35. After adjusting the $\chi(\alpha)$ function for each model to match the peak scattering intensities to a universal function at various $N \gtrsim 10^1$, the authors were able to obtain the universal phase behavior of models. However, for the aforementioned models with symmetric $z(N)$-distribution, the agreement between $\rho NS^{-1}(q^*)(\chi N)$ dependencies at a similar $\bar{N}$ and for different N can be reached without the fitting procedure and by using the simplest linear approximation for χ (Figure 5b). We suppose that this is the possible reason of why these two models exhibited similar $(\chi N)_{ODT}$ values and χN-dependencies of the excess free energy per chain (Figure 3). Based on these observations, we also propose that the peak scattering intensities could agree at the same $\bar{N}$ and χN for *all* models with symmetric $z(N)$-distributions using the $\chi = z\alpha/k_BT$ approximation, since the majority of the studied models belonging to this class had higher $\bar{N}$ and/or ρ than the models in Figures 4, 5 (Table S1). This could explain the existence of the master $(\chi N)_{ODT}(\bar{N})$ curve in Figure 2a. The rigorous confirmation of this hypothesis requires readjustment of all studied models with symmetric $z(N)$-distributions to obtain clusters of models having almost the same $\bar{N}$ as done in refs 5, 16, and 21 ($\bar{N}$ should coincide for all models in each cluster better than exhibited by the clusters of models in Figure 2a). After this, those models should be simulated at several χN values in the range $\chi N \in [0, (\chi N)_{ODT})$ and the $\rho NS^{-1}(q^*)(\chi N)$ dependencies should be measured, which is beyond the scope of this paper and is an interesting direction for future research.

We summarize the parameters of the studied DPD models having symmetric $z(N)$-distributions in Table 2. All these models have phase behavior (ODT point, free energy function) that depends only on the two parameters $\bar{N}$ and χN if the Flory–Huggins parameter χ is calculated as $\chi = z\alpha/k_BT$, where z is determined using ROL theory as done in this work and refs 5 and 21 (see SI section 2 for details). For comparison, we have also calculated the effective coordination number z following the broadly used mean-field approach developed by Groot and Warren;[12] we denoted this number as z_{liquid}. In this technique, one replaces a polymer melt with a binary liquid of monomers having the same a_{xx} and ρ and fits the density profiles at different degrees of separation to the predictions of the Flory–Huggins theory (Figure S5). Table 2 shows that most systems have the values of z that deviate significantly from the mean-field z_{liquid} parameter; z differs less than 5% from z_{liquid} only in a few FJC models. The calculation of z_{liquid} does not take the correlation hole effect into account, which leads to the discrepancy between z and z_{liquid}.[22] We suggest to use the ROL theory-derived parameter z for construction of the block copolymer phase diagrams; the $\chi = z\alpha/k_BT$ mapping will allow to compare the models with symmetric $z(N)$-distributions to each other or to experiment.

Table 2. Simple Linear Calibration of the Flory–Huggins Parameter $\chi = z\alpha/k_BT$ in the Studied DPD Models with Symmetric $z(N)$-Distributions[a]

ρ	K	r_0	a_{xx}	z	z_{liquid}
3	100	1.0	25.0	0.2837	0.2938
5	100	1.0	15.0	0.6607	0.6957
5	100	1.18	15.0	0.7024	0.6957
5	100	1.26	15.0	0.7120	0.6957
8	100	1.0	9.375	1.2612	1.3263
10	100	1.0	7.5	1.6707	1.7546
10	100	0.76745	7.5	1.5089	1.7546
10	100	1.14873	7.5	1.7167	1.7546
10	100	1.31	7.5	1.7433	1.7546
15	100	1.0	5.0	2.7040	2.8244
20	100	1.0	3.75	3.7443	3.8048
3	4.0	0.0	25.0	0.2193	0.2938
5	4.0	0.0	15.0	0.5479	0.6957
8	4.0	0.0	9.375	1.1090	1.3263
10	4.0	0.0	7.5	1.5014	1.7546
15	4.0	0.0	5.0	2.5099	2.8244
3	3.406	0.0	25.0	0.2363	0.2938

[a] z and z_{liquid} are the effective coordination numbers determined from ROL theory and from the mean-field fitting to the Flory–Huggins theory, respectively.

4. DISCUSSION AND CONCLUSIONS

The distribution of $z(N)$ characterizes the microscopic fluctuations of the potential energy of a monomer in a melt. The skewness of $z(N)$-distribution is mostly controlled by the model density ρ; the $z(N)$-distribution becomes symmetric when ρ exceeds a certain characteristic value, $\rho \gtrsim 3$ for DPD models with nonultrashort bonds. On the other hand, primarily for low-ρ models, the $z(N)$-distribution becomes skewed and leads to a poorly defined average value of z that no longer coincides with the most probable z. Therefore, the $\chi = z\alpha/k_BT$ approximation becomes most likely inapplicable to such models and leads to nonuniversal behavior. A better measure of a skewed distribution's "average" is its median; by finding z from the median values of $z(N)$, we found that transition points for all models agreed better with the master $(\chi N)_{ODT}(\bar{N})$ curve (Figure S3). Moreover, the data showed agreement with the master curve within the uncertainty associated with the difference between the mean, median, and

https://doi.org/10.1021/acs.macromol.4c00680
Macromolecules 2024, 57, 8212–8222

the mode of the skewed $z(N)$-distributions. Any of those three quantities can be a plausible measure of the "average" value of $z(N)$ used to calculate z; if the $z(N)$-distribution is symmetric, all of them coincide. Therefore, the models with symmetric $z(N)$-distributions do not have the nonuniversal model-dependent discrepancy between the average, the mode, and the median of the $z(N)$-distribution; in such models, the parameter z becomes "well-defined", representing both the average and the most frequent effective coordination numbers in a system. This, in turn, makes those models structurally similar to each other and to a hypothetical model with infinite ρ, in which the $z(N)$-distribution skewness is predicted to be also zero (SI section 6). For the latter model, in turn, the linear $\chi \propto \alpha$ formula is exact due to the vanishingly small α near ODT as predicted by the lattice cluster theory[17−20] and the ROL theory[22] (since $a_{xx} \propto 1/\rho$ at constant compressibility, see SI section 1). As a result, the similarity of different models with symmetric $z(N)$-distributions to each other and to the $\rho \to \infty$ model has presumably led to the coincidence of the normalized peak scattering intensity at the same $\bar{N}$ and χN for the models belonging to this class in the $\chi \propto \alpha$ approximation (Figure 5b). This, in turn, could lead to the existence of the $(\chi N)_{\mathrm{ODT}}(\bar{N})$ master curve in Figure 2a and to the free energy depending only on χN and $\bar{N}$ for this class of models (Figure 3) when $\chi \propto \alpha$ is assumed. However, a complete theoretical explanation of this effect is still lacking and is an interesting topic for future research.

What is the significance of the $z(N)$-distribution skew? In general, one expects the distribution of the coordination number to be skewed if the local liquid structure is important. For such models, this structure changes with α so significantly that the universality of all models can be achieved apparently only by adding nonlinear terms to the $\chi(\alpha)$ function. As a result, as shown in Figure 2b, the linear $\chi \propto \alpha$ approximation is not universally applicable for *all* models with $10^2 < \bar{N} < 10^4$, leading to the consistent behavior of only a *class* of models. At such values of $\bar{N}$, the nonlinear terms in the $\chi(\alpha)$ function are permitted in principle.[17−22] These fitting-based nonlinear terms can be calculated solely by fitting the *mesoscale* structure of the melt (peak of the structure factor) at different values of α as opposed to the *microscopically* determined characteristic z, which defines the linear part of $\chi(\alpha)$ and is calculated in the *homopolymer* melt state (i.e., at $\alpha = 0$). The authors of refs 5 and 21 did not assign a particular physical meaning to each of the nonlinear terms; instead, they were introduced to reach the agreement between the normalized peak scattering intensities measured in different models at the same $\bar{N}$ and χN. As Figure 5b suggests, these terms may be not necessary to reach this agreement between the models having symmetric $z(N)$-distributions, which could be the cause of the consistent phase behavior of those models in the linear approximation (Figure 2a, 3). How those nonlinear terms arise from skewed $z(N)$-distributions, how they depend on its characteristics, and what microscopic mechanism gives rise to the universal Morse et al. curve (eq 2) after inclusion of those nonlinearities are still unsolved questions and are promising topics for future research. However, the nonlinear terms in the $\chi(\alpha)$ expression help ROL theory to describe strong fluctuations at high α;[13] this theory, in turn, contains the universal description of all polymer models and, we believe, "accounts" for the $z(N)$-distribution skew.

To conclude, we discovered that a broad class of symmetric diblock copolymer melt models has phase behavior (phase transition points and free energies) depending only on $\bar{N}$ and χN in the linear $\chi = z\alpha/k_B\mathrm{T}$ approximation. This class includes the models with symmetric distribution of the monomer interaction potential energy $z(N)$ (i.e., the models with a well-defined value of z). The linear approximation for χ has a clear physical interpretation and *does not use any phenomenological fitting-based parameters*, since the coefficient z is an analytically defined characteristic of a homopolymer melt. The values of z in the studied DPD models with symmetric $z(N)$-distributions are summarized in Table 2. In addition, the models in which $z(N)$ is distributed symmetrically yielded the master $(\chi N)_{\mathrm{ODT}}(\bar{N})$ curve agreeing qualitatively with the FH scaling (eq 1). This simple definition of χ and the existence of the master $(\chi N)_{\mathrm{ODT}}(\bar{N})$ curve in the experimentally relevant range $\bar{N} > 10^2$ will allow researchers to compare the results of simulations to each other and to experiments without performing the complex and resource-demanding nonlinear Morse calibration for a broad class of models. In addition, we expect that models of block copolymers having different architecture will have consistent phase behavior in the $\chi \propto \alpha$ approximation if the $z(N)$-distribution is symmetric; this is the matter of our next study. As a final note, we would like to point out that FJC models having symmetric $z(N)$-distributions are particularly suitable for reverse mapping onto atomistic models of real polymer systems, since one can map a Kuhn segment to a bead of an FJC model, and the resulting model will have typical densities high enough to yield a symmetric $z(N)$-distribution. This might be quite beneficial for experimental and computational polymer scientists interested in block copolymer mesostructure design and polymer phase behavior.

■ ASSOCIATED CONTENT

Supporting Information

The Supporting Information is available free of charge at https://pubs.acs.org/doi/10.1021/acs.macromol.4c00680.

Additional simulation details, procedures of parameter determination, the theory describing skewness of the $z(N)$-distribution, and additional data supporting claims in the main text (PDF)

■ AUTHOR INFORMATION

Corresponding Authors

Artem Petrov − *Department of Chemical Engineering, Massachusetts Institute of Technology, Cambridge, Massachusetts 02139, United States*; orcid.org/0000-0002-1238-3745; Email: aipetrov@mit.edu

Alfredo Alexander-Katz − *Department of Materials Science and Engineering, Massachusetts Institute of Technology, Cambridge, Massachusetts 02139, United States*; Email: aalexand@mit.edu

Author

Hejin Huang − *Department of Materials Science and Engineering, Massachusetts Institute of Technology, Cambridge, Massachusetts 02139, United States*

Complete contact information is available at: https://pubs.acs.org/10.1021/acs.macromol.4c00680

Notes

The authors declare no competing financial interest.

https://doi.org/10.1021/acs.macromol.4c00680
Macromolecules 2024, 57, 8212−8222

■ ACKNOWLEDGMENTS

We thank Gabriella La Cour, Tianyi Jin, YongJoo Kim, Jian Qin, Mark Matsen, and Alexey Gavrilov for help and fruitful discussions. We acknowledge the MIT SuperCloud and Lincoln Laboratory Supercomputing Center for providing computational resources. This research was supported by the National Science Foundation through award number DMREF 2118678.

■ REFERENCES

(1) Sinturel, C.; Bates, F. S.; Hillmyer, M. A. High χ-low N block polymers: how far can we go? *ACS Macro Lett.* **2015**, *4*, 1044−1050.
(2) Helfand, E. Block copolymer theory. III. Statistical mechanics of the microdomain structure. *Macromolecules* **1975**, *8*, 552−556.
(3) Leibler, L. Theory of microphase separation in block copolymers. *Macromolecules* **1980**, *13*, 1602−1617.
(4) Grzywacz, P.; Qin, J.; Morse, D. C. Renormalization of the one-loop theory of fluctuations in polymer blends and diblock copolymer melts. *Phys. Rev. E* **2007**, *76*, 061802.
(5) Medapuram, P.; Glaser, J.; Morse, D. C. Universal phenomenology of symmetric diblock copolymers near the order-disorder transition. *Macromolecules* **2015**, *48*, 819−839.
(6) Brazovskii, S. Phase transition of an isotropic system to a nonuniform state. *J. Exp. Theor. Phys.* **1975**, *41*, 85.
(7) Fredrickson, G. H.; Helfand, E. Fluctuation effects in the theory of microphase separation in block copolymers. *J. Chem. Phys.* **1987**, *87*, 697−705.
(8) Mayes, A.; De La Cruz, M. O. Concentration fluctuation effects on disorder-order transitions in block copolymer melts. *J. Chem. Phys.* **1991**, *95*, 4670−4677.
(9) Bates, F. S.; Rosedale, J. H.; Fredrickson, G. H. Fluctuation effects in a symmetric diblock copolymer near the order-disorder transition. *J. Chem. Phys.* **1990**, *92*, 6255−6270.
(10) Bates, F. S.; Rosedale, J. H.; Fredrickson, G. H.; Glinka, C. J. Fluctuation-induced first-order transition of an isotropic system to a periodic state. *Physical review letters* **1988**, *61*, 2229.
(11) Rosedale, J. H.; Bates, F. S.; Almdal, K.; Mortensen, K.; Wignall, G. D. Order and disorder in symmetric diblock copolymer melts. *Macromolecules* **1995**, *28*, 1429−1443.
(12) Groot, R. D.; Warren, P. B. Dissipative particle dynamics: Bridging the gap between atomistic and mesoscopic simulation. *J. Chem. Phys.* **1997**, *107*, 4423−4435.
(13) Qin, J.; Morse, D. C. Fluctuations in symmetric diblock copolymers: Testing theories old and new. *Physical review letters* **2012**, *108*, 238301.
(14) Willis, J.; Beardsley, T.; Matsen, M. Calibration of a lattice model for high-molecular-weight block copolymer melts. *J. Chem. Phys.* **2019**, *150*, 204906.
(15) Vorselaars, B.; Stasiak, P.; Matsen, M. W. Field-theoretic simulation of block copolymers at experimentally relevant molecular weights. *Macromolecules* **2015**, *48*, 9071−9080.
(16) Glaser, J.; Qin, J.; Medapuram, P.; Müller, M.; Morse, D. C. Test of a scaling hypothesis for the structure factor of disordered diblock copolymer melts. *Soft Matter* **2012**, *8*, 11310−11317.
(17) Pesci, A. I.; Freed, K. F. Lattice models of polymer fluids: Monomers occupying several lattice sites. II. Interaction energies. *J. Chem. Phys.* **1989**, *90*, 2003−2016.
(18) Pesci, A. I.; Freed, K. F. Lattice theory of polymer blends and liquid mixtures: Beyond the Flory-Huggins approximation. *J. Chem. Phys.* **1989**, *90*, 2017−2026.
(19) Dudowicz, J.; Freed, K. F.; Madden, W. G. Role of molecular structure on the thermodynamic properties of melts, blends, and concentrated polymer solutions: comparison of Monte Carlo simulations with the cluster theory for the lattice model. *Macromolecules* **1990**, *23*, 4803−4819.
(20) Dudowicz, J.; Freed, M. S.; Freed, K. F. Effect of monomer structure and compressibility on the properties of multicomponent polymer blends and solutions. 2. Application to binary blends. *Macromolecules* **1991**, *24*, 5096−5111.
(21) Glaser, J.; Medapuram, P.; Beardsley, T. M.; Matsen, M. W.; Morse, D. C. Universality of block copolymer melts. *Physical review letters* **2014**, *113*, 068302.
(22) Morse, D. C.; Chung, J. K. On the chain length dependence of local correlations in polymer melts and a perturbation theory of symmetric polymer blends. *J. Chem. Phys.* **2009**, *130*, 224901.
(23) Müller, M.; Binder, K. Computer simulation of asymmetric polymer mixtures. *Macromolecules* **1995**, *28*, 1825−1834.
(24) Zong, J.; Wang, Q. Fluctuation/correlation effects in symmetric diblock copolymers: On the order-disorder transition. *J. Chem. Phys.* **2013**, *139*, 124907.
(25) Beardsley, T.; Spencer, R.; Matsen, M. Computationally efficient field-theoretic simulations for block copolymer melts. *Macromolecules* **2019**, *52*, 8840−8848.
(26) Beardsley, T.; Matsen, M. Calibration of the Flory-Huggins interaction parameter in field-theoretic simulations. *J. Chem. Phys.* **2019**, *150*, 174902.
(27) Qin, J.; Morse, D. C. Renormalized one-loop theory of correlations in polymer blends. *J. Chem. Phys.* **2009**, *130*, 224902.
(28) Qin, J.; Grzywacz, P.; Morse, D. C. Renormalized one-loop theory of correlations in disordered diblock copolymers. *J. Chem. Phys.* **2011**, *135*, 084902.
(29) Huang, H.; Alexander-Katz, A. Dissipative particle dynamics for directed self-assembly of block copolymers. *J. Chem. Phys.* **2019**, *151*, 154905.
(30) Jiao, G.-S.; Li, Y.; Qian, H.-J.; Lu, Z.-Y. Computer simulation study of polydispersity effect on the phase behavior of short diblock copolymers. *Polymer* **2016**, *96*, 6−12.
(31) Petrov, A.; Chertovich, A. V.; Gavrilov, A. A. Phase Diagrams of Polymerization-Induced Self-Assembly Are Largely Determined by Polymer Recombination. *Polymers* **2022**, *14*, 5331.
(32) Beardsley, T. M.; Matsen, M. W. Well-tempered metadynamics applied to field-theoretic simulations of diblock copolymer melts. *J. Chem. Phys.* **2022**, *157*, 114902.
(33) Zong, J.; Wang, Q. On the order-disorder transition of compressible diblock copolymer melts. *J. Chem. Phys.* **2015**, *143*, 184903.
(34) Gavrilov, A. A.; Chertovich, A. V. Polymerization-Induced Microphase Separation with Long-Range Order in Melts of Gradient Copolymers. *Polymers* **2020**, *12*, 2637.
(35) Glaser, J.; Qin, J.; Medapuram, P.; Morse, D. C. Collective and single-chain correlations in disordered melts of symmetric diblock copolymers: Quantitative comparison of simulations and theory. *Macromolecules* **2014**, *47*, 851−869.
(36) Gu, W.; Huh, J.; Hong, S. W.; Sveinbjornsson, B. R.; Park, C.; Grubbs, R. H.; Russell, T. P. Self-assembly of symmetric brush diblock copolymers. *ACS Nano* **2013**, *7*, 2551−2558.
(37) Marques, D. S.; Vainio, U.; Chaparro, N. M.; Calo, V. M.; Bezahd, A. R.; Pitera, J. W.; Peinemann, K.-V.; Nunes, S. P. Self-assembly in casting solutions of block copolymer membranes. *Soft Matter* **2013**, *9*, 5557−5564.
(38) Ziolek, R. M.; Omar, J.; Hu, W.; Porcar, L.; Gonzalez-Gaitano, G.; Dreiss, C. A.; Lorenz, C. D. Understanding the pH-directed self-assembly of a four-arm block copolymer. *Macromolecules* **2020**, *53*, 11065−11076.
(39) Berezkin, A. V.; Jung, F.; Posselt, D.; Smilgies, D. M.; Papadakis, C. M. Vertical vs lateral macrophase separation in thin films of block copolymer mixtures: computer simulations and GISAXS experiments. *ACS Appl. Mater. Interfaces* **2017**, *9*, 31291−31301.
(40) Gavrilov, A. A. Effect of the counterion size on microphase separation in charged-neutral diblock copolymers. *J. Chem. Phys.* **2023**, *158*, 054901.
(41) Groot, R. D.; Madden, T. J. Dynamic simulation of diblock copolymer microphase separation. *J. Chem. Phys.* **1998**, *108*, 8713−8724.

https://doi.org/10.1021/acs.macromol.4c00680
Macromolecules 2024, 57, 8212−8222

(42) Matsen, M. W. The standard Gaussian model for block copolymer melts. *J. Phys.: Condens. Matter* **2002**, *14*, R21.
(43) Alexander-Katz, A.; Fredrickson, G. H. Diblock copolymer thin films: A field-theoretic simulation study. *Macromolecules* **2007**, *40*, 4075−4087.
(44) Pike, D. Q.; Detcheverry, F. A.; Müller, M.; de Pablo, J. J. Theoretically informed coarse grain simulations of polymeric systems. *J. Chem. Phys.* **2009**, *131*, 084903.
(45) Detcheverry, F. A.; Kang, H.; Daoulas, K. C.; Müller, M.; Nealey, P. F.; De Pablo, J. J. Monte Carlo simulations of a coarse grain model for block copolymers and nanocomposites. *Macromolecules* **2008**, *41*, 4989−5001.
(46) Daoulas, K. C.; Müller, M. Single chain in mean field simulations: Quasi-instantaneous field approximation and quantitative comparison with Monte Carlo simulations. *J. Chem. Phys.* **2006**, *125*, 184904.
(47) Grest, G. S.; Lacasse, M.-D.; Kremer, K.; Gupta, A. M. Efficient continuum model for simulating polymer blends and copolymers. *J. Chem. Phys.* **1996**, *105*, 10583−10594.
(48) Wijesekera, A.; Vigil, D. L.; Ge, T. Molecular Simulations Revealing Effects of Non-concatenated Ring Topology on Phase Behavior of Symmetric Diblock Copolymers. *Macromolecules* **2024**, *57*, 5092−5104.

https://doi.org/10.1021/acs.macromol.4c00680
Macromolecules 2024, 57, 8212−8222